

GROUPED TRANSFORMATIONS IN HIGH-DIMENSIONAL EXPLAINABLE ANOVA APPROXIMATION

FELIX BARTEL*, DANIEL POTTS†, AND MICHAEL SCHMISCHKE‡

Abstract. In this paper we propose a tool for high-dimensional approximation based on trigonometric polynomials where we allow only low-dimensional dimension interactions. In a general high-dimensional setting it is already possible to deal with special sampling sets such as sparse grids or rank-1 lattices. This requires black-box access to the function, i.e., the ability to evaluate it at any point. Here, we focus on scattered data points and corresponding grouped frequency sets along the dimensions. From there we propose a fast matrix-vector multiplication, the grouped Fourier transform, that finds theoretical foundation in the context of the analysis of variance (ANOVA) decomposition where there is a one-to-one correspondence from the ANOVA terms to our proposed groups. We tested two different approximation approaches: Classical Tikhonov-regularization, namely, regularized least squares and the technique of group lasso, which promotes sparsity in the groups. As for the latter, there are no explicit solution formulas which is why we applied the fast iterative shrinkage-thresholding algorithm to obtain the minimizer. Numerical experiments in under-, overdetermined, and noisy settings indicate the applicability of our algorithms.

Key words. analysis of variance, ANOVA, explainable approximation, fast iterative shrinkage-thresholding algorithm, FISTA, group lasso, high dimensional approximation, multivariate trigonometric polynomials, nonequispaced fast Fourier transform, NFFT, LSQR

AMS subject classifications. 65T, 42B05

1. Introduction. Discrete transformations like the discrete Fourier transform, the discrete cosine transform, and many others play an important role in a large variety of applications in applied mathematics and other sciences. They have since given rise to algorithms like the fast Fourier transform (FFT) and the fast cosine transform that allow for the fast multiplication of the associated matrices, cf. [15]. The FFT with its many applications belongs to the most important algorithms of our time. Those concepts have been generalized to allow for nodes to be nonequispaced resulting in the nonequispaced fast Fourier transform (NFFT) and the nonequispaced fast cosine transform, cf. [9, 15]. While those algorithms have a good complexity, it depends on the size of the frequency index set which grows exponentially in the dimension for many common examples.

For high dimensional approximation with trigonometric polynomials there already exist efficient methods for special sampling grids, such as sparse grids [5, 7, 4] or rank-1 lattice nodes [8]. In [16] the multivariate analysis of variance (ANOVA) decomposition, cf. [11, 6], was related to a decomposition in the frequency domain that allowed for the Fourier coefficients to be considered in certain groups related to the ANOVA terms. If one assumes sparsity in the index sets related to sparsity in the number of groups, it is possible to decompose high-dimensional nonequispaced discrete transforms into multiple transforms associated with ANOVA terms. In this paper, we introduce the grouped Fourier transformation which is able to handle high-dimensional frequency index sets if they have sparsity in their support, i.e., the number of nonzero elements in the frequencies is limited by the so called superposition

*Chemnitz University of Technology, Germany (felix.bartel@math.tu-chemnitz.de, <http://www.tu-chemnitz.de/~febar/>).

†Chemnitz University of Technology, Germany (potts@math.tu-chemnitz.de, <http://www.tu-chemnitz.de/~potts/>).

‡Chemnitz University of Technology, Germany (michael.schmischke@math.tu-chemnitz.de, <http://www.tu-chemnitz.de/~mischmi/>).

dimension, cf. [16].

From these frequency index sets, we find a one-to-one relation to the truncated ANOVA decomposition which we use for approximation. In practical terms, we assume that the variables of a function only interact in low-dimensional groups or couplings. This yields a grouped frequency set which can be handled by the grouped Fourier transform. Moreover, we use sensitivity analysis, cf. [13], in order to rank the influence of the dimension interactions. This can be displayed or interpreted as an explainable ANOVA network. One main advantage of the Fourier approach is that we are able to immediately compute an approximation to the variance of the ANOVA terms.

We approach this problem in two different ways: The first method uses least-squares minimization with the LSQR algorithm, see [14]. As proposed in [16], in this paper we added a Tikhonov regularization term where we use Sobolev-weights to adapt our algorithm for different decay properties of the Fourier coefficients. When we know that the solution is sparse in the dimension interactions we can use the second method: the group lasso approach, cf. [20], which immediately promotes sparsity in the groups. This leads to a non-linear minimization problem, which we solve by using the fast iterative shrinking-thresholding Algorithm (FISTA), cf. [2]. To our knowledge this regularization was only done for ℓ_2 -norms for groups, but we were able to also use Sobolev-type norms in this setting. Even though one obtains good approximation errors from this already, one could restrict the active sets further and start LSQR again to obtain an even better approximation error, cf. [16].

The paper is organized as follows: We introduce the grouped Fourier transform for frequency sets of a grouped structure in Section 2 and propose a fast algorithm to compute it. Furthermore, we discuss complexity as well as the error of this algorithm. In Section 3 we reiterate on the ANOVA decomposition for periodic functions as previously discussed in [16]. We apply the grouped Fourier transform in Section 4 to the problem of approximating high-dimensional functions. This breaks down to solving least-squares problems of type (4.2). In the Subsection 4.1 we add a standard regularization term and therein use information about the smoothness of the function. The solver in this case is the well-known LSQR method, cf. [14]. Subsection 4.2 contains the group lasso regularization idea using FISTA, see Algorithm 4.1, as a solver. Here, the idea to use smoothness information is considered as well. We provide numerical examples with a special test function for both methods.

2. Grouped Fourier Transform. The discrete Fourier transformation in $d \in \mathbb{N}$ dimensions is given by

$$f_{\mathbf{x}} = \sum_{\mathbf{k} \in \mathcal{I}} \hat{f}_{\mathbf{k}} e^{2\pi i \langle \mathbf{k}, \mathbf{x} \rangle}$$

for $\mathbf{x} \in \mathcal{X}$, where $\mathcal{X} \subseteq \mathbb{T}^d$ is a fine set of nodes, $\mathcal{I} \subseteq \mathbb{Z}^d$ a frequency index set, and $\langle \cdot, \cdot \rangle$ the Euclidean inner product. The related Fourier matrix is given by

$$\mathbf{F}(\mathcal{X}, \mathcal{I}) = \left(e^{2\pi i \langle \mathbf{k}, \mathbf{x} \rangle} \right)_{\mathbf{x} \in \mathcal{X}, \mathbf{k} \in \mathcal{I}} \in \mathbb{C}^{|\mathcal{X}| \times |\mathcal{I}|},$$

where a straightforward matrix-vector multiplication requires $\mathcal{O}(|\mathcal{X}| |\mathcal{I}|)$ arithmetical operations.

The grouped Fourier transform is a special case where the frequency index set consists of a disjoint union of lower dimensional equispaced frequency index sets with zeros along some dimensions. It was first used as a tool in [16]. In this section we

introduce all necessities to carry out the computations in lower dimensions instead of the high spatial dimension. This will peak in the identity (2.1), which is then used to develop fast algorithms.

For a rigorous formulation, we introduce the following notation. The set of coordinate indices $\{1, \dots, d\}$ will be denoted by \mathcal{D} . For a vector $\mathbf{v} = (v_1, \dots, v_d)^\top$ and $\mathbf{u} \subseteq \mathcal{D}$ we define

$$\mathbf{v}_{\mathbf{u}} := (v_j)_{j \in \mathbf{u}} \in \mathbb{C}^{|\mathbf{u}|}$$

the restriction of \mathbf{v} to the dimensions in \mathbf{u} . Similarly, we use the same notation for sets in an elementwise fashion, i.e., for a set \mathcal{A} with d -dimensional elements we define

$$\mathcal{A}_{\mathbf{u}} := \{\mathbf{v}_{\mathbf{u}} : \mathbf{v} \in \mathcal{A}\}.$$

With that notation, we now introduce various useful frequency sets. We start with the one-dimensional frequency set $\mathcal{I}_N := \mathbb{Z} \cap [-N/2, N/2)$, $N \in 2\mathbb{N}$ and

$$\mathcal{I}_{\mathbf{N}}^d := \{\mathbf{k} \in \mathbb{Z}^d : k_j \in \mathcal{I}_{N_j} \text{ for } j \in \mathcal{D}\}$$

the multivariate cube with bandwidths $\mathbf{N} = (N_1, \dots, N_d)^\top \in (2\mathbb{N})^d$. Next, we introduce frequency sets along certain axis. For that, let $\mathbf{u} \subseteq \mathcal{D}$ and $\mathbf{N} \in 2\mathbb{N}^{|\mathbf{u}|}$. We then define

$$\mathcal{I}_{\mathbf{N}}^{\mathbf{u},d} := \{\mathbf{k} \in \mathcal{I}_{\mathbf{N}}^d : k_j = 0 \text{ for } j \in \mathcal{D} \setminus \mathbf{u} \text{ and } k_j \neq 0 \text{ for } j \in \mathbf{u}\}$$

where $\mathcal{I}_{\mathbf{N}}^{\emptyset,d} := \{\mathbf{0}\}$ by convention.

Remark 2.1. (i) We have $(\mathcal{I}_{\mathbf{N}}^{\mathbf{u},d})_{\mathbf{u}} = \times_{j \in \mathbf{u}} (\mathcal{I}_{N_j} \setminus \{0\})$ and, thus, we obtain for the cardinality $|\mathcal{I}_{\mathbf{N}}^{\mathbf{u},d}| = \prod_{j \in \mathbf{u}} (N_j - 1)$.

(ii) We can decompose $\mathcal{I}_{\mathbf{N}}^d$ by the following disjoint union

$$\mathcal{I}_{\mathbf{N}}^d = \bigcup_{\mathbf{u} \subseteq \mathcal{D}} \mathcal{I}_{\mathbf{N}}^{\mathbf{u},d}.$$

The above identity is visualized in [Figure 1](#).

With this notation we are ready for

DEFINITION 2.2. Let U be a subset of $\mathcal{P}(\mathcal{D})$, where \mathcal{P} stands for the powerset. For $\mathbf{u} \in U$, let $\mathbf{N}(\mathbf{u}) \in 2\mathbb{N}^{|\mathbf{u}|}$ be vectors of bandwidths and $\hat{f}_{\mathbf{k}} \in \mathbb{C}$ Fourier coefficients for $\mathbf{k} \in \mathcal{I}_{\mathbf{N}(\mathbf{u})}^{\mathbf{u},d}$. The grouped Fourier transform is then defined by

$$f_{\mathbf{x}} = \sum_{\mathbf{u} \in U} \sum_{\mathbf{k} \in \mathcal{I}_{\mathbf{N}(\mathbf{u})}^{\mathbf{u},d}} \hat{f}_{\mathbf{k}} e^{2\pi i \langle \mathbf{k}, \mathbf{x} \rangle}$$

for $\mathbf{x} \in \mathcal{X}$.

Computing the grouped Fourier transform from [Definition 2.2](#) via the naive approach, i.e., setting up the Fourier matrix $\mathbf{F}(\mathcal{X}, \mathcal{I})$ for

$$\mathcal{I} = \bigcup_{\mathbf{u} \in U} \mathcal{I}_{\mathbf{N}(\mathbf{u})}^{\mathbf{u},d}$$

and doing a matrix-vector multiplication with $\hat{\mathbf{f}} = (\hat{f}_{\mathbf{u}})_{\mathbf{u} \in U}$ results in the complexity class

$$\mathcal{O} \left(|\mathcal{X}| \sum_{\mathbf{u} \in U} |\mathcal{I}_{\mathbf{N}(\mathbf{u})}^{\mathbf{u},d}| \right) = \mathcal{O} \left(|\mathcal{X}| \sum_{\mathbf{u} \in U} \prod_{j \in \mathbf{u}} ((N(\mathbf{u}))_j - 1) \right).$$

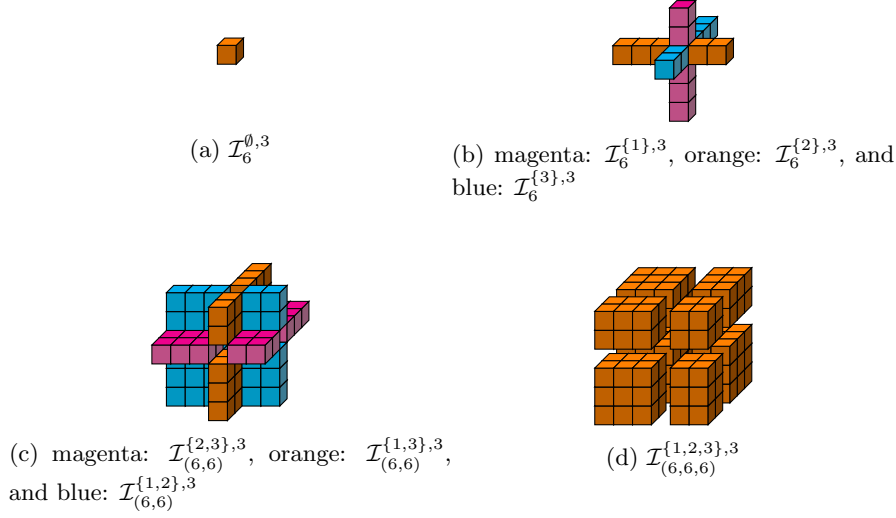


Fig. 1: Decomposition of $\mathcal{I}_{(6,6,6)}^3$ into its groups.

This is unfeasible but can be reduced as follows. Firstly, we observe that we are working with a block matrix, i.e.,

$$\mathbf{F}(\mathcal{X}, \mathcal{I}) = \left(\mathbf{F}^\top \left(\mathcal{X}, \mathcal{I}_{\mathbf{N}(\mathbf{u})}^{\mathbf{u},d} \right) \right)_{\mathbf{u} \in U}^\top.$$

Using the sparse structure of $\mathcal{I}_{\mathbf{N}(\mathbf{u})}^{\mathbf{u},d}$ we obtain

$$\begin{aligned} \mathbf{F} \left(\mathcal{X}, \mathcal{I}_{\mathbf{N}(\mathbf{u})}^{\mathbf{u},d} \right) &= \left(e^{2\pi i \langle \mathbf{k}, \mathbf{x} \rangle} \right)_{\mathbf{x} \in \mathcal{X}, \mathbf{k} \in \mathcal{I}_{\mathbf{N}(\mathbf{u})}^{\mathbf{u},d}} \\ &= \left(e^{2\pi i \langle \mathbf{k}, \mathbf{x}_{\mathbf{u}} \rangle} \right)_{\mathbf{x} \in \mathcal{X}, \mathbf{k} \in \times_{j \in \mathbf{u}} (\mathcal{I}_{(\mathbf{N}(\mathbf{u}))_j} \setminus \{0\})}. \end{aligned}$$

For $\hat{\mathbf{f}}(\mathbf{u})$ with frequency domain $\mathcal{I}_{\mathbf{N}(\mathbf{u})}^{\mathbf{u},d}$ we now introduce an extension such that the coefficients corresponding to zero-frequencies are filled with zeros and the frequency-dimension is reduced to $|\mathbf{u}|$. Thus, we have frequencies in $\mathcal{I}_{\mathbf{N}(\mathbf{u})}^{|\mathbf{u}|}$. This extension is visualized in Figure 2 and can be achieved formally by $\hat{\mathbf{g}}(\mathbf{u}) = ((\hat{\mathbf{g}}(\mathbf{u}))_{\mathbf{k}})_{\mathbf{k} \in \mathcal{I}_{\mathbf{N}(\mathbf{u})}^{|\mathbf{u}|}}$ with

$$(\hat{\mathbf{g}}(\mathbf{u}))_{\mathbf{k}_{\mathbf{u}}} = (\hat{\mathbf{f}}(\mathbf{u}))_{\mathbf{k}_{\mathbf{u}}}$$

for $\mathbf{k} \in \mathcal{I}_{\mathbf{N}(\mathbf{u})}^{\mathbf{u},d}$ and zero otherwise.

With that we have the identity

$$(2.1) \quad \mathbf{F} \left(\mathcal{X}, \mathcal{I}_{\mathbf{N}(\mathbf{u})}^{\mathbf{u},d} \right) \hat{\mathbf{f}}(\mathbf{u}) = \mathbf{F} \left(\mathcal{X}_{\mathbf{u}}, \mathcal{I}_{\mathbf{N}(\mathbf{u})}^{|\mathbf{u}|} \right) \hat{\mathbf{g}}(\mathbf{u}),$$

where the left-hand side operates in d dimensions and the right-hand side in $|\mathbf{u}|$ dimensions. Furthermore, the right-hand side of the above equation can be computed via the NFFT with the complexity $\mathcal{O}(\mathbf{N}(\mathbf{u})^{|\mathbf{u}|} \log \mathbf{N}(\mathbf{u}) + |\log \varepsilon|^{|\mathbf{u}|} |\mathcal{X}|)$. It follows

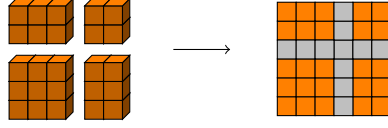


Fig. 2: Visualization of the extension for $\mathcal{I}_{(6,6)}^{\{2,3\},3}$ to $\mathcal{I}_{(6,6)}^2$.

that the multiplication with \mathbf{F} can be accomplished in

$$\mathcal{O}\left(\sum_{\mathbf{u} \in \mathcal{U}} \left(N(\mathbf{u})^{|\mathbf{u}|} \log N(\mathbf{u}) + |\log \varepsilon|^{|\mathbf{u}|} |\mathcal{X}|\right)\right)$$

by the NFFT for precision ε .

Remark 2.3. For an error estimate we have for the NFFT

$$\left| \sum_{\mathbf{k} \in \mathcal{I}_{N(\mathbf{u})}^{\mathbf{u},d}} \hat{f}_{\mathbf{k}} e^{2\pi i \langle \mathbf{k}, \mathbf{x} \rangle} - \text{NFFT}(\hat{\mathbf{g}}(\mathbf{u})) \right| \leq C_{\mathbf{u}}(N(\mathbf{u})) \|\hat{\mathbf{f}}(\mathbf{u})\|_1$$

where $C_{\mathbf{u}}(N(\mathbf{u}))$ decays exponentially in $N(\mathbf{u})$, cf. [15, Theorem 7.8] and references therein. Since the grouped Fourier transform is simply a sum of the above, we can bound the overall error by

$$\left(\max_{\mathbf{u} \in \mathcal{U}} C_{\mathbf{u}}(N(\mathbf{u})) \right) \|\hat{\mathbf{f}}\|_1.$$

Remark 2.4. The considerations in this section are not limited to the exponential functions, but rather, can be extended to any orthonormal basis. In fact, for $\exp(2\pi i \langle \mathbf{k}, \cdot \rangle)$ and $\cos(\pi \langle \mathbf{k}, \cdot \rangle)$ the presented ideas are already implemented in the julia package `GroupedTransforms` which can be found on GitHub, see github.com/NFFT/GroupedTransforms, where the nonequispaced fast cosine transform (NFCT) is used for performance in the latter.

3. ANOVA Decomposition. In this section we discuss the main properties of the *ANOVA decomposition*, see [3, 11, 6], for periodic functions. For a more detailed description we refer to [16].

Every function $f \in L_2(\mathbb{T}^d)$ has a unique ANOVA decomposition which is defined as

$$f = \sum_{\mathbf{u} \subseteq \mathcal{D}} f_{\mathbf{u}}$$

with ANOVA terms

$$f_{\mathbf{u}}(\mathbf{x}) := \sum_{\substack{\mathbf{k} \in \mathbb{Z}^d \\ \text{supp } \mathbf{k} = \mathbf{u}}} c_{\mathbf{k}}(f) e^{2\pi i \langle \mathbf{k}, \mathbf{x} \rangle}$$

where $c_{\mathbf{k}}(f) = \int_{\mathbb{T}^d} f(\mathbf{x}) e^{-2\pi i \langle \mathbf{k}, \mathbf{x} \rangle} d\mathbf{x}$ are the Fourier coefficients and $\text{supp } \mathbf{k} = \{j \in \mathcal{D} : k_j \neq 0\}$. In order to measure the importance of an ANOVA term $f_{\mathbf{u}}$ in relation to the function f , we use *global sensitivity indices*

$$(3.1) \quad \varrho(\mathbf{u}, f) := \frac{\sigma^2(f_{\mathbf{u}})}{\sigma^2(f)} \quad \text{with} \quad \sigma^2(f) := \|f\|_{L_2(\mathbb{T}^d)}^2 - |c_0(f)|^2,$$

cf. [18, 19, 11]. This motivates the concept of effective dimensions. The superposition dimension is a particular effective dimension and is given as the smallest integer $d_s \in \mathcal{D}$ such that

$$\sum_{\substack{\mathbf{u} \subseteq \mathcal{D} \\ |\mathbf{u}| \leq d_s}} \sigma^2(f_{\mathbf{u}}) \geq \alpha \sigma^2(f)$$

for some $\alpha \in [0, 1]$. This means that the variance of the function can mostly be explained by up to d_s -dimensional couplings in the variables.

The number of ANOVA terms is 2^d and therefore grows exponentially in the dimension which reflects the well-known curse of dimensionality. In order to circumvent this, it is a good idea to truncate the ANOVA decomposition and only take a certain number of terms into account. A subset of ANOVA terms is a set $U \subseteq \mathcal{P}(\mathcal{D})$ such that U is downward closed, i.e., if \mathbf{u} is an element of U , all subsets $\mathbf{v} \subseteq \mathbf{u}$ are also elements of U . A special truncation possibility is motivated by the superposition dimension $d_s \in \mathcal{D}$. Forming the set of terms of at most d_s variables

$$(3.2) \quad U_{d_s} = \{\mathbf{u} \subseteq \mathcal{D} : |\mathbf{u}| \leq d_s\},$$

we define the truncation

$$\mathbb{T}_{d_s} f := \sum_{\mathbf{u} \in U_{d_s}} f_{\mathbf{u}}.$$

To obtain finite dimensions, we truncate a second time in that we make the frequency sets finite. We achieve this in the following way: Let

$$\mathcal{I}^{\mathbf{u}, d} = \{\mathbf{k} \in \mathbb{Z}^d : \omega_{\mathbf{u}}(\mathbf{k}_{\mathbf{u}}) \leq N_{\mathbf{u}} \text{ and } \mathbf{k}_j = 0 \text{ for } j \notin \mathbf{u}\}$$

for weight functions $\omega_{\mathbf{u}} : \mathbb{Z}^{|\mathbf{u}|} \rightarrow [0, \infty)$, integers $N_{\mathbf{u}}$, and $\mathbf{u} \in U$. These sets correspond to the ANOVA terms defined by $\mathbf{u} \subseteq \mathcal{D}$. We then set $\mathcal{I} = \bigcup_{\mathbf{u} \in U_{d_s}} \mathcal{I}^{\mathbf{u}, d}$ such that for every $\mathbf{k} \in \mathcal{I}$ it holds that $\|\mathbf{k}\|_0 \leq d_s$. The corresponding Fourier partial sum is then defined as

$$(3.3) \quad S_{\mathcal{I}} f(\mathbf{x}) = \sum_{\mathbf{k} \in \mathcal{I}} c_{\mathbf{k}}(f) e^{2\pi i \langle \mathbf{k}, \mathbf{x} \rangle}.$$

4. Approximation. In this section, we consider the problem of approximating periodic functions $f : \mathbb{T}^d \rightarrow \mathbb{C}$ with high spatial dimension $d \in \mathbb{N}$. In particular, we consider a scattered data setting where our given data about the unknown function f are sampling values $\mathbf{y} = (f(\mathbf{x}))_{\mathbf{x} \in \mathcal{X}}$ on a finite set of nodes $\mathcal{X} \subseteq \mathbb{T}^d$. We are looking for an approximation of the Fourier partial sum (3.3) of the truncated ANOVA decomposition and want to incorporate the fast algorithms from Section 2. If only ANOVA terms of an order up to a small $d_s \in \mathcal{D}$ occur in f this truncation leads to a reasonable model. In particular, we will use the ANOVA terms $f_{\mathbf{u}}$, $\mathbf{u} \in U_{d_s}$, from (3.2) with full frequency grids

$$\mathcal{I} = \bigcup_{\mathbf{u} \in U_{d_s}} \mathcal{I}_{N(\mathbf{u})}^{\mathbf{u}, d}$$

and the bandwidths $N(\mathbf{u}) \in (2\mathbb{N})^{|\mathbf{u}|}$, see Section 2. Since the Fourier coefficients $c_{\mathbf{k}}(f) \in \mathbb{C}$ are not known, we are going to approximate them by coefficients $\hat{f}_{\mathbf{k}} \approx c_{\mathbf{k}}(f)$

that we determine from the given data \mathcal{X} and \mathbf{y} . We obtain an approximate Fourier partial sum

$$S_{\mathcal{I}}^{\mathcal{X}} f(\mathbf{x}) := \sum_{\mathbf{k} \in \mathcal{I}} \hat{f}_{\mathbf{k}} e^{2\pi i \mathbf{k} \cdot \mathbf{x}}$$

with $\hat{f}_{\mathbf{k}} \in \mathbb{C}$ such that $S_{\mathcal{I}}^{\mathcal{X}} f(\mathbf{x}) \approx S_{\mathcal{I}} f(\mathbf{x})$. The two goals are to detect which of the ANOVA terms $f_{\mathbf{u}}$ for $\mathbf{u} \in U$ are of a high-importance to the function and simultaneously achieve a small approximation error

$$(4.1) \quad \frac{\|f - S_{\mathcal{I}}^{\mathcal{X}} f\|_{L_2(\mathbb{T}^d)}}{\|f\|_{L_2(\mathbb{T}^d)}}.$$

This problem was considered in [16] with the idea of solving least-squares minimization problems of the type

$$(4.2) \quad \min_{\hat{\mathbf{f}}} \|\mathbf{y} - \mathbf{F}(\mathcal{X}, \mathcal{I}) \hat{\mathbf{f}}\|_2^2$$

in order to determine the approximate coefficients $\hat{f}_{\mathbf{k}} \in \mathbb{C}$. From them, we can calculate the global sensitivity indices (3.1) via Parseval's identity for a so-called attribute ranking which is of a high relevance in numerous applications.

In [Subsection 4.1](#) we reiterate on the approach presented in [16] which uses the LSQR method to tackle problem (4.2). We are going to extend this approach by adding a standard regularization term known from the ordinary Tikhonov regularization, but simultaneously consider weights which incorporate information about the decay rate in the Fourier coefficients. In particular we use weights corresponding to functions from a Sobolev type space

$$H^{\omega}(\mathbb{T}^d) := \left\{ f \in L_2(\mathbb{T}^d) : \|f\|_{H^{\omega}(\mathbb{T}^d)} := \sqrt{\sum_{\mathbf{k} \in \mathbb{Z}^d} \omega^2(\mathbf{k}) |c_{\mathbf{k}}(f)|^2} < \infty \right\}$$

for a weight function $\omega: \mathbb{Z}^d \rightarrow [1, \infty)$, cf. [10, 16].

[Subsection 4.2](#) introduces an approach that promotes sparsity of the groups in U_{d_s} via regularization and is based on the group lasso technique, cf. [20]. As in the prior case, Sobolev weights will be used in this section as well.

Both sections use iterative solvers which require fast multiplication with $\mathbf{F}(\mathcal{X}, \mathcal{I})$ and its adjoint which is provided by the grouped Fourier transform from [Section 2](#).

For comparability reasons we work with the same test function throughout this paper

$$(4.3) \quad f: [-1, 1]^9 \rightarrow \mathbb{R}, \\ \mathbf{x} \mapsto B_2(x_1)B_4(x_3)B_6(x_8) + B_2(x_2)B_4(x_5)B_6(x_6) + B_2(x_4)B_4(x_7)B_6(x_9),$$

where B_2 , B_4 and B_6 are parts of univariate, shifted, scaled, and dilated B-splines of order 2, 4, and 6, respectively. Their Fourier series is given by

$$B_j(x) := c_j \sum_{k \in \mathbb{Z}} \operatorname{sinc}^j\left(\frac{\pi \cdot k}{j}\right) \cos(\pi \cdot k) e^{2\pi i k \cdot x} \quad \text{for } j = 2, 4, 6,$$

with $\text{sinc}(x) := \sin(x)/x$ and the constants $c_2 := \sqrt{3/4}$, $c_4 := \sqrt{315/604}$, $c_6 := \sqrt{277200/655177}$ such that $\|B_j\|_{L_2(\mathbb{T})} = 1$. This allows the direct computation of the Fourier coefficients $c_{\mathbf{k}}(f)$ and the norm $\|f\|_{L_2(\mathbb{T}^d)}$. Moreover, the function has dominating-mixed smoothness of $3/2 - \varepsilon$ for every $\varepsilon > 0$, i.e., $f \in H^{\omega_\varepsilon}(\mathbb{T}^9)$ with

$$\omega_\varepsilon(\mathbf{k}) = \prod_{j \in \text{supp } \mathbf{k}} (1 + |k_j|)^{\frac{3}{2} - \varepsilon},$$

cf. [17]. The ANOVA terms $f_{\mathbf{u}}$ are only nonzero for

$$(4.4) \quad \mathbf{u} \in U^* := \mathcal{P}(\{1, 3, 8\}) \cup \mathcal{P}(\{2, 5, 6\}) \cup \mathcal{P}(\{4, 7, 9\})$$

which is one information we aim to find. The function f therefore has an exact low-dimensional structure for $d_s = 3$, i.e., can be represented by at most three-dimensional ANOVA terms or, in other words, variable couplings. This leads to $d_s = 3$ being the optimal choice for the superposition dimension with no error caused by the ANOVA truncation. Of course, in the approximation scenario the function f that generates our data is not known.

4.1. LSQR. The general approximation approach using LSQR is described in detail in [16] together with error estimates for functions in Sobolev type spaces. Here, we want to add a regularization idea using additional a-priori information about the decay of the Fourier coefficients. We achieve this by a weight function $\omega: \mathbb{Z}^d \rightarrow [1, \infty)$ such that $|c_{\mathbf{k}}(f)| \in \mathcal{O}(\omega^{-1}(\mathbf{k}))$, which relates to the function having some kind of smoothness. In order to incorporate this information we add a regularization term to (4.2) and obtain the problem

$$(4.5) \quad \min_{\hat{\mathbf{f}}} \left\| \mathbf{y} - \mathbf{F}(\mathcal{X}, \mathcal{I}) \hat{\mathbf{f}} \right\|_2^2 + \lambda \left\| \hat{\mathbf{f}} \right\|_{\hat{\mathbf{W}}}^2$$

with the weighted norm $\|\hat{\mathbf{f}}\|_{\hat{\mathbf{W}}}^2 = \hat{\mathbf{f}}^H \hat{\mathbf{W}} \hat{\mathbf{f}}$ and $\hat{\mathbf{W}} = \text{diag}(\omega(\mathbf{k}))_{\mathbf{k} \in \mathcal{I}}$ a diagonal matrix.

We apply the method with our minimization problem (4.5) to the test function (4.3) which we sample at 10 000 uniform i.i.d. random nodes on \mathbb{T}^9 and use the Sobolev weights

$$(4.6) \quad \omega(\mathbf{k}) = \prod_{j=1}^9 (1 + |k_j|)^s$$

for $s \geq 0$ in $\hat{\mathbf{W}}$. In the following numerical experiments we apply our method with a maximal iteration count of 50 for different parameters s and $\mathbf{N}(\mathbf{u})$ as well as a range of $\lambda > 0$. The results are always plotted with the L_2 -error and the global sensitivity indices (3.1) for each $|\mathbf{u}| = 1, 2, 3$ separately.

- (i) In the first setting we chose $\omega(\mathbf{k}) = 1$ for all $\mathbf{k} \in \mathcal{I}$, which penalizes all frequencies equally. The regularization term in (4.5) then becomes a standard ℓ_2 regularization. To compensate for the lack of information we chose relatively small bandwidths

$$(4.7) \quad \mathbf{N}(\mathbf{u}) = \begin{cases} (64) & \text{for } |\mathbf{u}| = 1 \\ (8, 8) & \text{for } |\mathbf{u}| = 2 \\ (4, 4, 4) & \text{for } |\mathbf{u}| = 3, \end{cases}$$

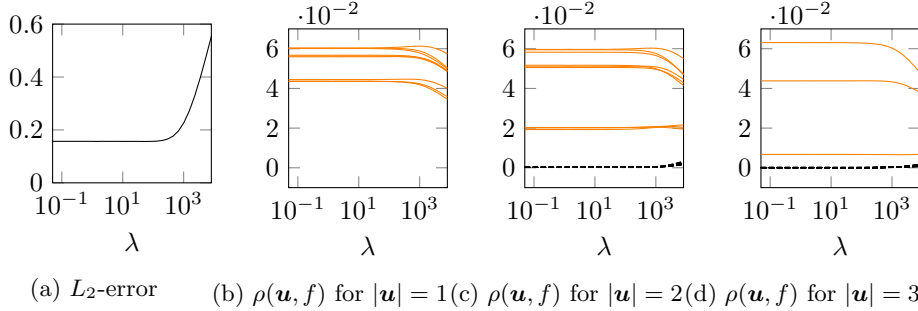


Fig. 3: LSQR with small bandwidths given in (4.7) on exact data with $s = 0$ (orange: active ANOVA terms U^* , dashed: inactive ANOVA terms in the test function).

which add up to 4600 frequencies such that we are in an overdetermined setting. The results of the LSQR approach to solving the minimization is depicted in Figure 3. The minimal relative L_2 -error is 0.156 which originates mostly from the very small bandwidths and can be improved to 0.122 by restarting the with the active set of couplings. Still, we are able to distinguish the global sensitivity indices of the active couplings very clearly from the ones not occurring in the test function. In (b) we observe that the global sensitivity indices $\rho(\mathbf{u}, f)$ are larger than zero for all nine one-dimensional ANOVA terms $f_{\mathbf{u}}$, $\mathbf{u} \in U^*$, $|\mathbf{u}| = 1$, occurring in the test function. The nine two-dimensional terms $f_{\mathbf{u}}$, $\mathbf{u} \in U^*$, $|\mathbf{u}| = 2$, are clearly separated from the inactive terms in $\mathcal{P}(\mathcal{D}) \setminus U^*$, see (c). The plot (d) shows that we can distinguish two of the active terms $f_{\mathbf{u}}$, $\mathbf{u} \in U^*$, $|\mathbf{u}| = 3$, clearly while one is still distinguishable yet closer to the inactive terms.

- (ii) In the next experiment we added 10% Gaussian noise which results in Figure 4. As expected, the minimal L_2 -error 0.515 is now larger, but can still be improved to 0.260 by restarting. We get the typical behaviour of under- and overfitting in the L_2 -error which can be recognized in the global sensitivity indices as well: For small λ the ANOVA terms $f_{\mathbf{u}}$ not occurring in the test function are not zero in our approximation since our approximation fits the noise. For large λ on the other hand we also penalize ANOVA terms $f_{\mathbf{u}}$ which actually occur in the test function as can be seen by the orange lines dropping. Overall, the active couplings are still distinguishable but for one ANOVA term in $|\mathbf{u}| = 3$ it becomes more difficult.
- (iii) To achieve a smaller L_2 -error we have to increase the bandwidths

$$(4.8) \quad \mathbf{N}(\mathbf{u}) = \begin{cases} (278) & \text{for } |\mathbf{u}| = 1 \\ (26, 26) & \text{for } |\mathbf{u}| = 2 \\ (8, 8, 8) & \text{for } |\mathbf{u}| = 3, \end{cases}$$

which results in 57856 frequencies such that we are underdetermined. With that many degrees of freedom we have to reduce our search space. We achieve that by using Sobolev weights (4.6) for $s = 2.5$ in $\hat{\mathbf{W}}(\mathbf{u})$ which propagate functions with respective decay in the Fourier coefficients. This is a higher smoothness than the function f itself has, but certain ANOVA terms decay faster since they are themselves splines of higher order or products of them.

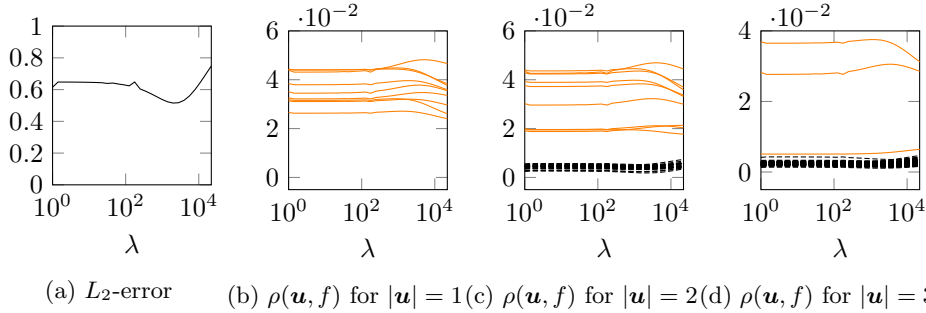


Fig. 4: LSQR with small bandwidths given in (4.7) on noisy data with $s = 0$ (orange: active ANOVA terms U^* , dashed: inactive ANOVA terms in the test function).

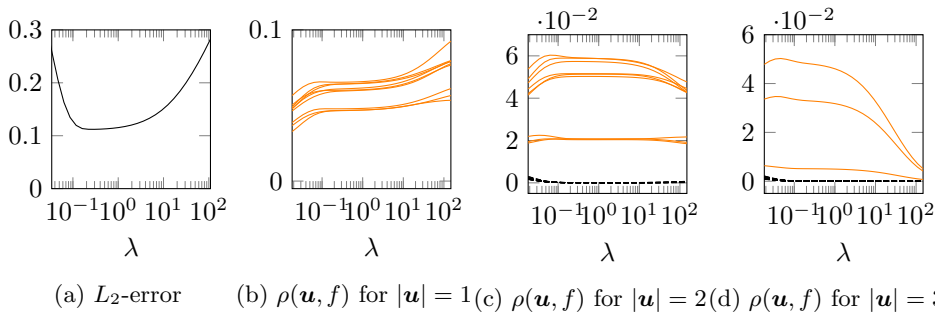


Fig. 5: LSQR with large bandwidths given in (4.8) on exact data with $s = 2.5$ (orange: active ANOVA terms U^* , dashed: inactive ANOVA terms in the test function).

The results for the experiment without noise are shown in Figure 5 and look very similar to the experiment with smaller bandwidths but the minimal L_2 -error is smaller: 0.112. It can be decreased down to $9.01 \cdot 10^{-3}$ by solving the problem with the active terms. The active ANOVA terms in U^* are clearly separable from the inactive ANOVA terms.

- (iv) The same experiment with 10% Gaussian noise can be seen in Figure 6. In comparison to the noisy experiment with small bandwidths we achieve a smaller minimal L_2 -error 0.300 with improvement down to 0.190. In addition the ANOVA term $f_{\mathbf{u}}$ for $|\mathbf{u}| = 3$ is now a little better distinguishable as the weights filter out the non-smooth noise.

Remark 4.1. Theorem 6.8 from [16] and [12] state that $\mathbb{E}(\mathbf{F}^H(\mathcal{X}, \mathcal{I})\mathbf{F}(\mathcal{X}, \mathcal{I})) = \mathbf{I}$ with \mathbb{E} being the expected value. This reasons the applicability of the methods in [1] which allow for the fast computation of the cross-validation score. This can then be used to choose a λ which will be close to the $L_2(\mathbb{T}^d)$ -optimal one, i.e., neither over- or underfitting, since the $L_2(\mathbb{T}^d)$ -error itself is not available in practical application scenarios.

4.2. Group Lasso. As it is promoted in Section 3, we often have a sparse structure in the groups $\mathbf{u} \in U$ but not so much within them. Thus, it comes natural

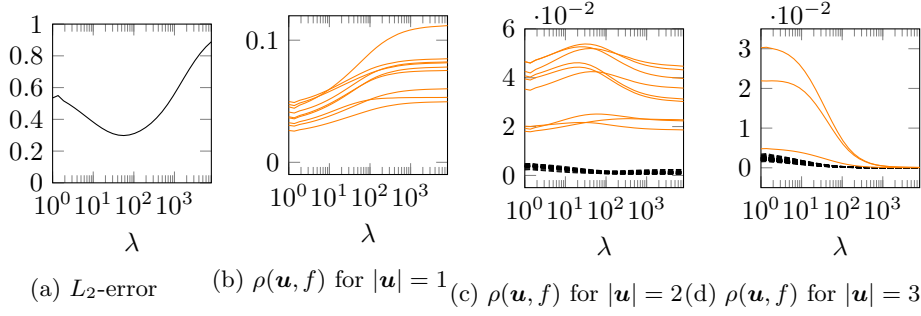


Fig. 6: LSQR with large bandwidths given in (4.8) on noisy data with $s = 2.5$ (orange: active ANOVA terms U^* , dashed: inactive ANOVA terms in the test function).

to work with the concept of group lasso, i.e., we seek the solution $\hat{\mathbf{f}}^*$ of

$$(4.9) \quad \min_{\hat{\mathbf{f}}} \frac{1}{2} \|\mathbf{y} - \mathbf{F}(\mathcal{X}, \mathcal{I})\hat{\mathbf{f}}\|_2^2 + \lambda \sum_{\mathbf{u} \in U} \|\hat{\mathbf{f}}(\mathbf{u})\|_{\hat{\mathbf{W}}(\mathbf{u})}$$

where we use the weighted norm $\|\hat{\mathbf{f}}(\mathbf{u})\|_{\hat{\mathbf{W}}(\mathbf{u})}^2 = \hat{\mathbf{f}}(\mathbf{u})^H \hat{\mathbf{W}}(\mathbf{u}) \hat{\mathbf{f}}(\mathbf{u})$ and $\hat{\mathbf{W}}(\mathbf{u}) = \text{diag}(\omega(\mathbf{k}))_{\mathbf{k} \in \mathcal{I}_{N(\mathbf{u})}^{u,d}}$ diagonal matrices with weight functions $\omega : \mathbb{Z}^d \rightarrow [1, \infty)$ for $\mathbf{u} \in U$. In contrast to Subsection 4.1, the regularization term has an ℓ_1 -norm structure around the groups and therefore pushes towards a small number of active couplings.

To address the non-smooth convex minimization problem (4.9) there are various proximal gradient methods. Entranced by the computational simplicity and quadratic rate of convergence, we use the fast iterative shrinking-thresholding algorithm (FISTA), cf. [2], as our algorithm of choice.

Algorithm 4.1 FISTA for group lasso

Input: $L_0 > 0$, $\eta > 1$, and $\hat{\mathbf{f}}_0$

Output: $\hat{\mathbf{f}}^*$ Minimizer of (4.9)

```

1:  $\hat{\mathbf{h}}_1 \leftarrow \hat{\mathbf{f}}_0$ ,  $t_1 \leftarrow 1$ 
2: for  $k = 1, \dots$  do
3:    $L_k \leftarrow L_{k-1}$ 
4:    $\hat{\mathbf{f}}_k \leftarrow p_{L_k}(\hat{\mathbf{h}}_k)$ 
5:   while  $\|\mathbf{y} - \mathbf{F}(\mathcal{X}, \mathcal{I})\hat{\mathbf{f}}_k\|_2^2 > \|\mathbf{y} - \mathbf{F}(\mathcal{X}, \mathcal{I})\hat{\mathbf{h}}_k\|_2^2 + 2\langle \hat{\mathbf{f}}_k - \hat{\mathbf{h}}_k, \mathbf{F}^H(\mathcal{X}, \mathcal{I})(\mathbf{F}(\mathcal{X}, \mathcal{I})\hat{\mathbf{h}}_k - \mathbf{y}) \rangle + L_k \|\hat{\mathbf{f}}_k - \hat{\mathbf{h}}_k\|_2^2$  do
6:      $L_k \leftarrow \eta L_k$ 
7:      $\hat{\mathbf{f}}_k \leftarrow p_{L_k}(\hat{\mathbf{h}}_k)$ 
8:   end while
9:    $t_{k+1} \leftarrow (1 + \sqrt{1 + 4t_k^2})/2$ 
10:   $\hat{\mathbf{h}}_{k+1} \leftarrow \hat{\mathbf{f}}_k + (t_k - 1)/(t_{k+1})(\hat{\mathbf{f}}_k - \hat{\mathbf{f}}_{k-1})$ 
11: end for

```

Algorithm 4.1 is the FISTA algorithm adopted to our setting, where $p_L(\hat{\mathbf{h}})$ is the

minimizer of

$$(4.10) \quad \frac{1}{2} \left\| \hat{\mathbf{f}} - \left(\hat{\mathbf{h}} - \frac{1}{L} \mathbf{F}^H(\mathcal{X}, \mathcal{I}) \left(\mathbf{F}(\mathcal{X}, \mathcal{I}) \hat{\mathbf{h}} - \mathbf{y} \right) \right) \right\|_2^2 + \frac{\lambda}{L} \sum_{\mathbf{u} \in U} \|\hat{\mathbf{f}}_{\mathbf{u}}\|_{\hat{\mathbf{W}}(\mathbf{u})}.$$

Remark 4.2. The computational most expensive part is the projection p_L which we will reduce to one multiplication with $\mathbf{F}(\mathcal{X}, \mathcal{I})$ and one with its adjoint. Note, that there is also a variant of the FISTA algorithm which uses constant step size L_k which makes the inner loop obsolete. For that, the complexity of the FISTA step boils down to the complexity of computing p_L . The quadratic convergence rate assures us, that a small number of iterations is sufficient.

To compute the projection p_L we develop an explicit formula, which will be done in the next theorem with the use of the following lemma.

LEMMA 4.3. *Let $\mathbf{x}_1^*(\lambda)$ and $\mathbf{x}_2^*(\xi)$ be the minimizers of*

$$\frac{1}{2} \|\mathbf{x} - \mathbf{y}\|_2^2 + \lambda \|\mathbf{x}\|_{\hat{\mathbf{W}}} \quad \text{and} \quad \|\mathbf{x} - \mathbf{y}\|_2^2 + \xi \|\mathbf{x}\|_{\hat{\mathbf{W}}},$$

respectively, for $\hat{\mathbf{W}} = \text{diag}(\omega(k))_{k \in \mathcal{I}}$, $\omega : \mathbb{Z}^d \rightarrow [0, \infty)$ and some index set \mathcal{I} . Then

(i) for $0 < \xi$ we have

$$\mathbf{x}_2^*(\xi) = \text{diag} \left(\frac{1}{1 + \xi \omega(k)} \right)_{k \in \mathcal{I}} \mathbf{y},$$

(ii) for $0 < \xi$ and

$$\lambda = \left\| \left(\frac{y_k}{1/\xi + \omega(k)} \right)_{k \in \mathcal{I}} \right\|_{\hat{\mathbf{W}}}$$

we have $\mathbf{x}_1^(\lambda) = \mathbf{x}_2^*(\xi)$, and*

(iii) for

$$\lambda \geq \left\| \left(\frac{y_k}{\omega(k)} \right)_{k \in \mathcal{I}} \right\|_{\hat{\mathbf{W}}}$$

we have $\mathbf{x}_1^(\lambda) = \mathbf{0}$.*

Proof. (i) We simply calculate the roots of the gradient

$$\mathbf{x} - \mathbf{y} + 2\xi \hat{\mathbf{W}} \mathbf{x} \stackrel{!}{=} \mathbf{0} \quad \Leftrightarrow \quad \mathbf{x}_2^*(\xi) = \text{diag} \left(\frac{1}{1 + \xi \omega(k)} \right)_{k \in \mathcal{I}} \mathbf{y}.$$

The convexity of the function assures the minimizing property.

(ii) Similarly to (i), computing $\mathbf{x}_1^*(\lambda)$ can be done by root-finding of

$$\nabla_{\mathbf{x}} \left(\frac{1}{2} \|\mathbf{x} - \mathbf{y}\|_2^2 + \lambda \|\mathbf{x}\|_{\hat{\mathbf{W}}} \right) = \mathbf{x} - \mathbf{y} + \frac{\lambda}{\|\mathbf{x}\|_{\hat{\mathbf{W}}}} \text{diag}(\omega(k))_{k \in \mathcal{I}} \mathbf{x}$$

since the function in question is strictly convex. Using the ansatz $\mathbf{x} = \mathbf{x}_2^*(\xi)$ and (i) leads to

$$\left(\text{diag} \left(\frac{1}{1 + \xi \omega(k)} \right)_{k \in \mathcal{I}} - \mathbf{I} + \frac{\lambda \text{diag} \left(\frac{\omega(k)}{1 + \xi \omega(k)} \right)_{k \in \mathcal{I}}}{\left\| \text{diag} \left(\frac{1}{1 + \xi \omega(k)} \right)_{k \in \mathcal{I}} \mathbf{y} \right\|_{\hat{\mathbf{W}}}} \right) \mathbf{y} \stackrel{!}{=} \mathbf{0}.$$

This is certainly fulfilled if the diagonal matrix is zero in each component, i.e.,

$$\frac{1}{1 + \xi\omega(k)} - 1 + \frac{\lambda}{\left\| \text{diag} \left(\frac{1}{1 + \xi\omega(k)} \right)_{k \in \mathcal{I}} \mathbf{y} \right\|_{\hat{\mathbf{W}}}} \frac{\omega(k)}{1 + \xi\omega(k)} \stackrel{!}{=} 0,$$

or equivalently,

$$\lambda \stackrel{!}{=} \left\| \text{diag} \left(\frac{1}{1/\xi + \omega(k)} \right)_{k \in \mathcal{I}} \mathbf{y} \right\|_{\hat{\mathbf{W}}}.$$

(iii) We want to minimize

$$\frac{1}{2} \|\mathbf{x} - \mathbf{y}\|_2^2 + \lambda \|\mathbf{x}\|_{\hat{\mathbf{W}}}.$$

Using polar coordinates we see that varying the arguments in \mathbf{x} does not change the second summand. Hence, \mathbf{x} and \mathbf{y} have to have the same arguments in each component. Without loss of generality, we restrict to the moduli of these numbers, i.e., positive numbers.

Then

$$\begin{aligned} \frac{1}{2} \|\mathbf{0} - \mathbf{y}\|_2^2 + \lambda \|\mathbf{0}\|_{\hat{\mathbf{W}}} &= \frac{1}{2} \|\mathbf{x} - \mathbf{x} + \mathbf{x} - \mathbf{y}\|_2^2 \\ &\leq \frac{1}{2} \|\mathbf{x} - \mathbf{y}\|_2^2 + \left\langle \text{diag} \left(\sqrt{\omega(k)} \right)_{k \in \mathcal{I}} \mathbf{x}, \text{diag} \left(\frac{1}{\sqrt{\omega(k)}} \right)_{k \in \mathcal{I}} \mathbf{y} \right\rangle. \end{aligned}$$

By the Cauchy-Schwarz inequality, we obtain

$$\frac{1}{2} \|\mathbf{0} - \mathbf{y}\|_2^2 + \lambda \|\mathbf{0}\|_2 \leq \frac{1}{2} \|\mathbf{x} - \mathbf{y}\|_2^2 + \|\mathbf{x}\|_{\hat{\mathbf{W}}} \left\| \text{diag} \left(1/\sqrt{\omega(k)} \right)_{k \in \mathcal{I}} \mathbf{y} \right\|_2.$$

Now making use of $\|\text{diag}(1/\sqrt{\omega(k)})_{k \in \mathcal{I}} \mathbf{y}\|_2 < \lambda$ we end up with

$$\frac{1}{2} \|\mathbf{0} - \mathbf{y}\|_2^2 + \lambda \|\mathbf{0}\|_2 \leq \frac{1}{2} \|\mathbf{x} - \mathbf{y}\|_2^2 + \lambda \|\mathbf{x}\|_{\hat{\mathbf{W}}}$$

which holds for all \mathbf{x} and, hence, $\mathbf{0}$ is the minimizer for this case. \square

Now, using [Lemma 4.3](#), we prove an explicit formula for the projection p_L defined via the minimizer of [\(4.10\)](#).

THEOREM 4.4. *Let U be a subset of $\mathcal{P}(\{1, \dots, d\})$ and $\hat{\mathbf{W}}(\mathbf{u}) = \text{diag}(\omega(k))_{k \in \mathcal{I}_{\mathbf{N}(\mathbf{u})}^{\mathbf{u}, d}}$ diagonal matrices with strictly positive weights for $\mathbf{u} \in U$. For any $\mathbf{y} \in \mathbb{C}^N$, $N = \sum_{\mathbf{u} \in U} \prod_{j \in \mathbf{u}} (1 - (\mathbf{N}(\mathbf{u}))_j)$, and $\lambda > 0$ the minimizer of*

$$\frac{1}{2} \|\mathbf{x} - \mathbf{y}\|_2^2 + \lambda \sum_{\mathbf{u} \in U} \|\mathbf{x}_{\mathbf{u}}\|_{\hat{\mathbf{W}}(\mathbf{u})}$$

is given by

$$\mathbf{x}_{\mathbf{u}}^* = \begin{cases} \text{diag} \left(\frac{1}{1 + \xi(\mathbf{u})\omega(k)} \right)_{k \in \mathcal{I}_{\mathbf{N}(\mathbf{u})}^{\mathbf{u}, d}} \mathbf{y} & \text{for } \lambda \leq \left\| \left(\frac{y_k}{\omega(k)} \right)_{k \in \mathcal{I}_{\mathbf{N}(\mathbf{u})}^{\mathbf{u}, d}} \right\|_{\hat{\mathbf{W}}(\mathbf{u})} \\ \mathbf{0} & \text{otherwise} \end{cases}$$

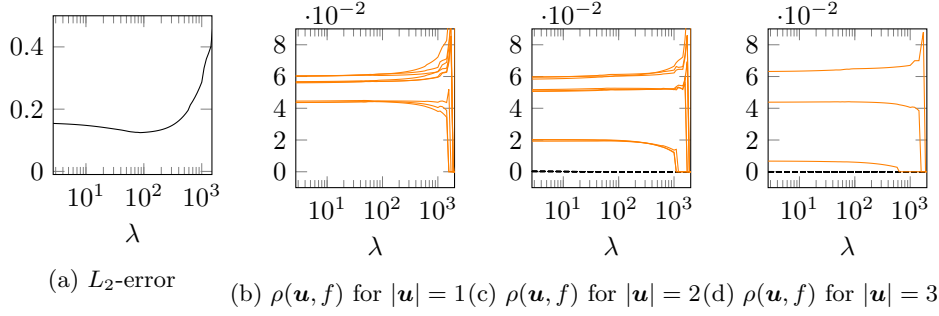


Fig. 7: FISTA with small bandwidths given in (4.7) on exact data with $s = 0$ (orange: active ANOVA terms U^* , dashed: inactive ANOVA terms in the test function).

for $\mathbf{u} \in U$ with $\xi(\mathbf{u})$ fulfilling

$$\left\| \left(\frac{y_k}{1/\xi(\mathbf{u}) + \omega(k)} \right)_{k \in \mathcal{I}_{N(\mathbf{u})}^{u,d}} \right\|_{\hat{\mathbf{W}}(\mathbf{u})} = \lambda.$$

Proof. Because of the structure of the objective function, we can minimize for every $\mathbf{u} \in U$ separately. Lemma 4.3 (i)-(iii) then results the assertion. \square

Remark 4.5. In Theorem 4.4 we still have to find $\xi(\mathbf{u})$ such that

$$t(\xi) := \left\| \left(\frac{y_k}{1/\xi(\mathbf{u}) + \omega(k)} \right)_{k \in \mathcal{I}_{N(\mathbf{u})}^{u,d}} \right\|_{\hat{\mathbf{W}}(\mathbf{u})}^2 = \lambda^2.$$

We do that in two steps:

- (i) Firstly we determine whether $t(1) \geq \lambda^2$ or not. If so, ξ has to be smaller than one because of the monotonicity of the objective function. Then we use the bisection method on $t(\cdot)$ with the initial interval $[0, 1]$. Otherwise we do the same for the function $t(1/\cdot)$.
- (ii) To obtain a more precise result we use some iterations with Newton's method afterwards.

Now for the numerical experiments. Again, we use the nine-dimensional function (4.3) which we sampled in 10 000 uniform i.i.d. random nodes on \mathbb{T}^9 . For four different settings we launched Algorithm 4.1 with 50 iterations and a range of λ . We started with the initial guess $\hat{\mathbf{f}}_0 = \mathbf{0}$ and the biggest λ as the minimizer $\hat{\mathbf{f}}^*(\lambda)$, presumably, is close to $\mathbf{0}$ for this case. For the other λ we used the last solution as new initial guess since $\hat{\mathbf{f}}^*(\lambda)$ depends continuously on λ . For evaluation we plotted the L_2 -error and the global sensitivity indices (3.1) for each $|\mathbf{u}| = 1, 2, 3$ separately.

- (i) In the first setting we chose $\omega(\mathbf{k}) = 1$ for all $\mathbf{k} \in \mathcal{I}$, which penalizes all frequencies equally, cf. Subsection 4.1. To compensate for the lack of information we chose relatively small bandwidths as in (4.7) such that we are in an overdetermined setting. The bandwidths are chosen such that each ANOVA term has the same amount of frequencies as otherwise group lasso would set smaller groups with fewer frequencies to zero for sparsity as data fitting is easier with groups of more degrees of freedom.

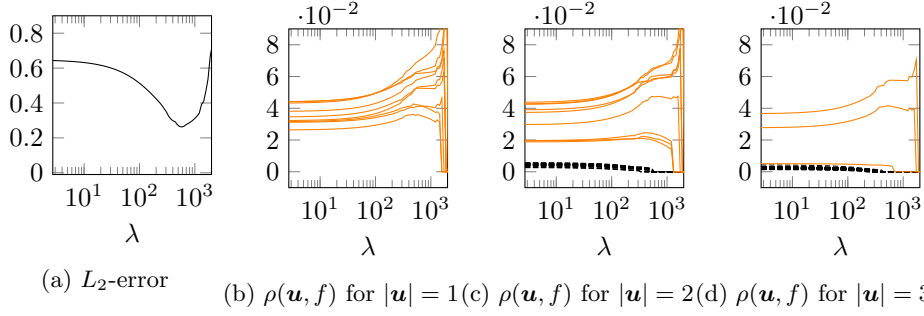


Fig. 8: FISTA with small bandwidths given in (4.7) on noisy data with $s = 0$ (orange: active ANOVA terms U^* , dashed: inactive ANOVA terms in the test function).

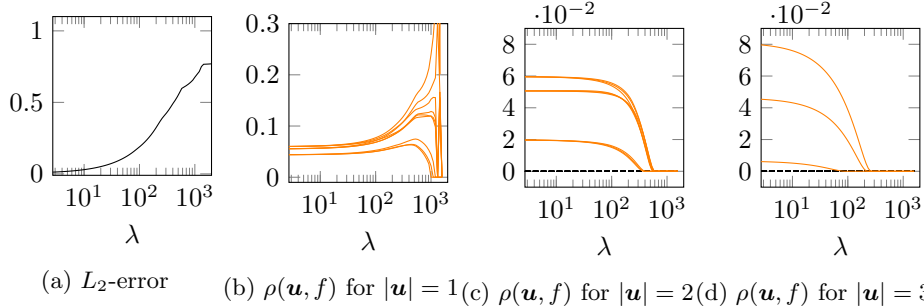


Fig. 9: FISTA with large bandwidths given in (4.8) on exact data with $s = 2.5$ (orange: active ANOVA terms U^* , dashed: inactive ANOVA terms in the test function).

The results of this first experiment without noise can be seen in Figure 7. The minimal relative L_2 -error is 0.125 which is similar to the observations in Subsection 4.1. Still, we are able to distinguish the global sensitivity indices of the active couplings very clearly from the ones not occurring in the test function. In (b) we observe that the global sensitivity indices $\rho(\mathbf{u}, f)$ are larger than zero for all one-dimensional ANOVA terms $f_{\mathbf{u}}$ occurring in the test function. In (c) and (d) we have a typical ℓ_1 -regularization behaviour, as many groups are penalized to be exactly zero, for larger λ even the ones which occur in the test function.

- (ii) In the next experiment we added 10% Gaussian noise which results in Figure 8. As expected, the minimal L_2 -error 0.262 is now larger. We observe the typical behaviour of under- and overfitting in the L_2 -error, see (a), which can be recognized in the global sensitivity indices as well: For small λ the ANOVA terms $f_{\mathbf{u}}$ not occurring in the test function are not zero in our approximation since our approximation fits the noise. For large λ on the other hand we also penalize ANOVA terms $f_{\mathbf{u}}$ which actually occur in the test function as can be seen by the orange lines dropping. Overall, the active couplings are still distinguishable but for one ANOVA term in $|\mathbf{u}| = 3$ it becomes more difficult.
- (iii) To achieve a smaller L_2 -error we have to increase the bandwidths to the same as in the LSQR experiment: (4.8) which results in 57 856 frequencies such that

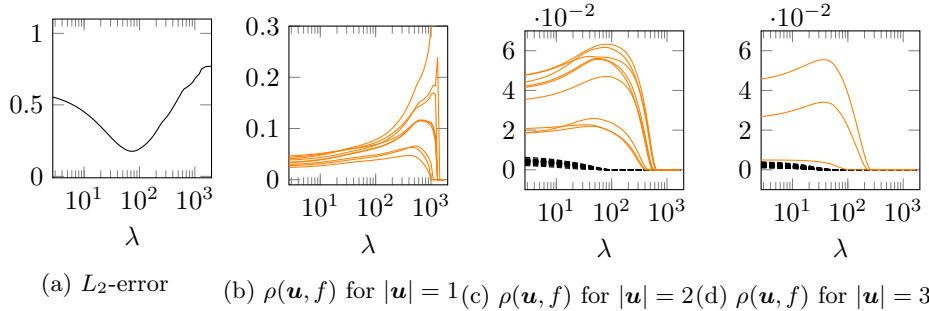


Fig. 10: FISTA with large bandwidths given in (4.8) on noisy data with $s = 2.5$ (orange: active ANOVA terms U^* , dashed: inactive ANOVA terms in the test function).

we are underdetermined. With that many degrees of freedom we have to reduce our search space. We achieve that by using Sobolev weights (4.6) for $s = 2.5$ in $\hat{\mathbf{W}}(\mathbf{u})$.

The results without noise can be seen in Figure 9. The results look very similar to the experiment with smaller bandwidths but the minimal L_2 -error is smaller: $1.240 \cdot 10^{-2}$. Furthermore, under- and overfitting does not occur as the L_2 -error curve is strictly increasing.

- (iv) The same experiment with 10% Gaussian noise can be seen in Figure 10. In comparison to the noisy experiment with small bandwidths we achieve a smaller minimal L_2 -error 0.199. In addition the ANOVA term $f_{\mathbf{u}}$ for $|\mathbf{u}| = 3$ is now a little better distinguishable as the weights filter out the non-smooth noise.

5. Conclusion. In the context of Fourier analysis, we introduced frequency index sets consisting of groups along lower-dimensional cubes in the frequency domain. These can then be used to move the computations from the original d dimensions to the dimension of the groups which are only of dimension up to a $d_s < d$. We presented a fast algorithm — the grouped Fourier transform — based on the identity (2.1). If these frequency index sets additionally have a grid-like structure along their axis we were able to carry out every matrix-vector multiplication via the nonequispaced fast Fourier transformation (NFFT) to obtain the typical FFT-like complexity.

Even though we assumed a very special structure, there is a proven application: We established an one-to-one correspondence to the ANOVA decomposition, which we briefly introduced. We then presented two approaches to compute an approximation of the truncated ANOVA decomposition by order of the terms or couplings.

- (i) The first method follows the concept of minimizing the Tikhonov-functional (4.5). This is an extension of the ideas in [16] which also manage noise and underdetermined settings.
- (ii) The second approach uses the group lasso idea, where we used the ANOVA terms for the groups (4.9). In contrast to the classical Tikhonov-regularization this promotes sparsity which underlies many applications. As there is no explicit formula for the solution of this non-smooth minimization problem, we used the FISTA algorithm to tackle this problem.

Both approaches performed well in the numerical results which cover under-, overdetermined, and also noisy settings. The code is available as julia package `ANOVAapprox`

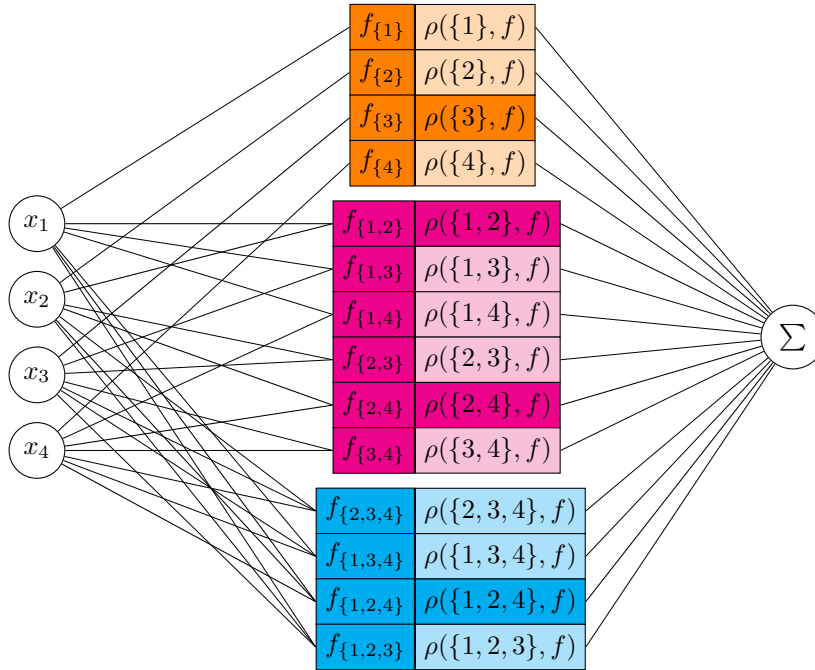


Fig. 11: Explainable ANOVA network of a function f for $d_s = 3$. We visualize the different ANOVA terms $f_{\mathbf{u}}$ for $|\mathbf{u}| = 1$ in orange, $|\mathbf{u}| = 2$ in magenta and for $|\mathbf{u}| = 3$ in blue. The related global sensitivity indices $\rho(\mathbf{u}, f)$ serve as interpretable quantity for the ANOVA term.

on GitHub, see <https://github.com/NFFT/ANOVAapprox>. As shown in [16], it is possible to work with a huge amount of data, namely multiple million nodes, using this methods. This would of course be a severely overdetermined setting. Moreover, is possible to apply the LSQR method again only for the active terms which improves the approximation result further.

Since we end up with a Fourier representation of the ANOVA decomposition, we can visualize it in the form of an explainable ANOVA network, see Figure 11. This representation immediately shows the couplings of the variables and, with help of the global sensitivity indices (3.1), depicts the importance of individual ANOVA terms or, in other words, which terms are active and which are not.

Acknowledgments. Felix Bartel acknowledges funding by the European Social Fund (ESF), Project ID 100367298. Daniel Potts acknowledges funding by the German Research Foundation (Deutsche Forschungsgemeinschaft) - Project ID 416228727 - SFB 1410.

REFERENCES

- [1] F. BARTEL, R. HIELSCHER, AND D. POTTS, *Fast cross-validation in harmonic approximation*, Applied and Computational Harmonic Analysis, 49 (2020), pp. 415–437, <https://doi.org/10.1016/j.acha.2020.05.002>.
- [2] A. BECK AND M. TEOULLE, *A fast iterative shrinkage-thresholding algorithm for linear inverse problems*, SIAM J. Imaging Sci., 2 (2009), pp. 183–202, <https://doi.org/10.1137/080716542>,

- <https://doi.org/10.1137/080716542>.
- [3] R. CAFLISCH, W. MOROKOFF, AND A. OWEN, *Valuation of mortgage-backed securities using Brownian bridges to reduce effective dimension*, J. Comput. Finance, 1 (1997), pp. 27–46, <https://doi.org/10.21314/jcf.1997.005>.
 - [4] M. GRIEBEL AND J. HAMAËKERS, *Fast discrete Fourier transform on generalized sparse grids*, in Sparse Grids and Applications - Munich 2012, J. Garcke and D. Pflüger, eds., vol. 97 of Lect. Notes Comput. Sci. Eng., Springer International Publishing, 2014, pp. 75–107, https://doi.org/10.1007/978-3-319-04537-5_4.
 - [5] M. HEGLAND, *Adaptive sparse grids*, in ANZIAM J, 2001, pp. 335–353, <https://doi.org/10.21914/anziamj.v44i0.685>.
 - [6] M. HOLTZ, *Sparse grid quadrature in high dimensions with applications in finance and insurance*, vol. 77 of Lecture Notes in Computational Science and Engineering, Springer-Verlag, Berlin, 2011, <https://doi.org/10.1007/978-3-642-16004-2>.
 - [7] Y. JIANG AND Y. XU, *Fast discrete algorithms for sparse Fourier expansions of high dimensional functions*, J. Complexity, 26 (2010), pp. 51–81.
 - [8] L. KÄMMERER, D. POTTS, AND T. VOLKMER, *Approximation of multivariate periodic functions by trigonometric polynomials based on rank-1 lattice sampling*, J. Complexity, 31 (2015), pp. 543–576, <https://doi.org/10.1016/j.jco.2015.02.004>.
 - [9] J. KEINER, S. KUNIS, AND D. POTTS, *Using NFFT3 - a software library for various nonequispaced fast Fourier transforms*, ACM Trans. Math. Software, 36 (2009), pp. Article 19, 1–30, <https://doi.org/10.1145/1555386.1555388>.
 - [10] T. KÜHN, S. MAYER, AND T. ULLRICH, *Counting Via Entropy: New Preasymptotics for the Approximation Numbers of Sobolev Embeddings*, SIAM J. Numer. Anal., 54 (2016), pp. 3625–3647, <https://doi.org/10.1137/16m106580x>.
 - [11] R. LIU AND A. B. OWEN, *Estimating Mean Dimensionality of Analysis of Variance Decompositions*, J. Amer. Statist. Assoc., 101 (2006), pp. 712–721, <https://doi.org/10.1198/016214505000001410>.
 - [12] M. MÖLLER AND T. ULLRICH, *Improved guarantees for least squares approximation in reproducing kernel Hilbert spaces*, ArXiv e-prints 000, (2020).
 - [13] J. E. OAKLEY AND A. O'HAGAN, *Probabilistic sensitivity analysis of complex models: a bayesian approach*, Journal of the Royal Statistical Society: Series B (Statistical Methodology), 66 (2004), pp. 751–769, <https://doi.org/10.1111/j.1467-9868.2004.05304.x>.
 - [14] C. C. PAIGE AND M. A. SAUNDERS, *LSQR: An algorithm for sparse linear equations and sparse least squares*, ACM Trans. Math. Software, 8 (1982), pp. 43–71, <https://doi.org/10.1145/355984.355989>.
 - [15] G. PLONKA, D. POTTS, G. STEIDL, AND M. TASCHE, *Numerical Fourier Analysis*, Applied and Numerical Harmonic Analysis, Birkhäuser, 2018, <https://doi.org/10.1007/978-3-030-04306-3>.
 - [16] D. POTTS AND M. SCHMISCHKE, *Approximation of high-dimensional periodic functions with Fourier-based methods*, ArXiv e-prints 1907.11412, (2019).
 - [17] D. POTTS AND T. VOLKMER, *Sparse high-dimensional FFT based on rank-1 lattice sampling*, Appl. Comput. Harmon. Anal., 41 (2016), pp. 713–748.
 - [18] I. M. SOBOL, *On sensitivity estimation for nonlinear mathematical models*, Keldysh Applied-Mathematics Institute, 1 (1990), pp. 112–118.
 - [19] I. M. SOBOL, *Global sensitivity indices for nonlinear mathematical models and their Monte Carlo estimates*, Math. Comput. Simulation, 55 (2001), pp. 271–280, [https://doi.org/10.1016/s0378-4754\(00\)00270-6](https://doi.org/10.1016/s0378-4754(00)00270-6).
 - [20] M. YUAN AND Y. LIN, *Model selection and estimation in regression with grouped variables*, J. R. Stat. Soc. Ser. B Stat. Methodol., 68 (2006), pp. 49–67, <https://doi.org/10.1111/j.1467-9868.2005.00532.x>, <https://doi.org/10.1111/j.1467-9868.2005.00532.x>.